Fatigue crack closure assessment by wavelet transform of infrared thermography signals

Lorenzo Bercelli, Bruno Levieil, Cédric Doudard, Sylvain Calloch

International Journal of Fatigue 190 (2025) 108639

Contents lists available at ScienceDirect

International Journal of Fatigue

journal homepage: www.elsevier.com/locate/ijfatigue

Fatigue crack closure assessment by wavelet transform of infrared thermography signals

Lorenzo Bercelli *, Bruno Levieil, Cédric Doudard, Sylvain Calloch

ENSTA Bretagne, IRDL – UMR CNRS 6027, 29200 Brest, France

ARTICLE INFO

Keywords:
Crack closure
Continuous wavelet transform
Thermoelastic stress analysis
Fatigue crack growth
Full-field measurement

ABSTRACT

The occurrence of crack closure significantly impacts the fatigue life of materials and structural components. Whether it is induced by the nature of the loading, the fabrication process or the geometry of the structure, its magnitude and effect should be considered to further improve predictive models of fatigue crack propagation. However, the definition of reliable experimental methods for the observation and assessment of fatigue crack closure, and in particular suited to structure testing, remains a challenge. The present study aims to provide a novel approach for the assessment of fatigue crack closure via the continuous wavelet transform of infrared thermography data. The processing of the temperature signal close to the crack in a coherent time–frequency space allows for the identification of crack closing and opening instants associated with high-frequency components. The method is meant to be suited to any testing configuration (conventional compact tension specimen or full-scale structures) with minimum operator-dependent parameters.

1. Introduction

Whether it is induced by plasticity, by crack faces roughness, by pre-existing residual stresses or by the nominal loading itself, the fatigue crack closure phenomenon [1] deeply affects the crack propagation rate and thus the fatigue life of the defective structure [2–5]. A conventional approach to consider the phenomenon of fatigue crack closure consists of defining an effective stress intensity range ΔK_{eff} that is less than the applied stress intensity range ΔK. It is defined as the difference between the maximum Stress Intensity Factor (SIF) K_{max} and the SIF at crack opening K_{op}, $\Delta K_{eff} = K_{max} - K_{op}$ (if $K_{op} > K_{\min}$). This effective stress intensity range then corresponds to the portion of the applied stress intensity range for which the crack is open, as crack closure is considered to shield the crack from further propagation. In the work by Elber [6], on a 2024-T3 aluminium alloy, a value of K_{op} is determined by assessing the nonlinearity of the compliance curve. It is suggested that K_{op} only depends on the stress ratio R and that the crack is either fully open ($\geq K_{op}$) or fully closed ($< K_{op}$). An empirical relationship $\Delta K_{eff} = U\Delta K$ with $U = 0.5 + 0.4R$ is then proposed (with R the stress ratio), where U is the effective stress range ratio. However, this threshold approach proposed by Elber was questioned by numerous subsequent studies on fatigue crack closure [7]. Indeed, experimental results suggested that a crack could propagate even below K_{op}. Moreover, it was shown that the measurement of K_{op} was very dependent on measurement location [8,9]. Other approaches to determine ΔK_{eff} were proposed, relying on the idea that partial closure only causes partial crack shielding. For instance, an elastic extrapolation of the compliance curve was made in the work by Chen et al. [10]; other studies introduced an effect of the crack wake [11–13]. A "hybrid" method [14] was also proposed, in which a partial crack closure approach is considered for long cracks, while the Elber approach is applied to physically short cracks. A recent discussion among researchers, initiated by Kujawski [15], suggests that the description of the effect of closure on fatigue crack growth and its measurement remains a challenge. In order to better understand this phenomenon, robust test procedures must be developed.

Experimental techniques for assessing crack closure can be distinguished into two categories, namely direct and indirect methods. Direct methods rely on the measurement of the distance between the crack faces (optical observation [16,17], electron microscope observation [18], X-ray tomography [19], …). Typical indirect methods include potential drop [20], acoustic emission [8] or near-crack tip gage measurement [6]. For a complete and detailed review of methods for crack closing assessment, the reader is invited to refer to the work by Stoychev and Kujawski [7]. In the field of indirect techniques, recent studies have proposed the use of infrared thermography to assess fatigue crack closure. In a previous work by the authors [4] on T-welded steel joints, the definition of an effective stress range $\Delta\sigma_{eff}$ was proposed by fitting

* Corresponding author.
E-mail address: lorenzo.bercelli@ensta-bretagne.fr (L. Bercelli).

https://doi.org/10.1016/j.ijfatigue.2024.108639
Received 17 July 2024; Received in revised form 26 September 2024; Accepted 4 October 2024
Available online 5 October 2024

Nomenclature

E	Young modulus
ν	Poisson coefficient
ρ	Density
c	Specific heat
α	Coefficient of thermal expansion
λ	Thermal conductivity
T_0	Initial temperature
$\vec{q}$	Local heat flux
Δ	Intrisic dissipation source
C_{the}	Thermoelastic coupling source
θ	Temperature variation
θ_d	Temperature linked to the intrisic dissipation
θ^a_{the}	Temperature linked to the thermoelastic coupling under adiabatic condition
θ^a_1	Amplitude of the temperature's first harmonic under adiabatic condition
θ_{the}	Temperature linked to the thermoelastic coupling considering conduction effects
θ_i	Amplitude of the temperature's i^{th} harmonic considering conduction effects
ϕ_i	Phase of the temperature's i^{th} harmonic considering conduction effects
R_{nom}	Nominal load ratio
F_a	Load amplitude
f_m	Mechanical frequency
f_c	Infrared camera sampling frequency
N	Number of loading cycles
l	Crack length
σ_{nom}	Nominal stress
$\Delta\sigma_{nom}$	Nominal stress range
$\Delta\sigma_{eff}$	Effective stress range
I_1	First invariant of the stress tensor
I_{1_a}	Amplitude of the first invariant of the stress tensor
τ_o	Effective stress range ratio
τ_o^{th}	Theoretical effective stress range ratio for a linear elastic case
t_o	Crack opening time within one loading cycle
c_n	Crack closing instant at cycle n
o_n	Crack opening instant at cycle n
$\psi_{a,b}$	Ricker type wavelet
a	Wavelet scale
b	Wavelet shift
s_{CWT}	Scalogram, result of the continuous wavelet transform
ϵ_{IR}	Noise standard deviation of the infrared data
θ_1^{th}	Theoretical value of the temperature's first harmonic amplitude at the applied nominal stress amplitude
n_h	Number of harmonics to be considered for the DCT reconstruction of the temperature signal
f_{DCT}	Sampling rate to be considered for the DCT reconstruction of the temperature signal
ϕ_{ref}	Reference phase of the temperature's first harmonic, away from the crack
θ_{the}^{DCT}	DCT reconstruction of the temperature linked to the thermoelastic coupling considering conduction effects
n_{RL}	Number of ridge lines detected in the scalogram
b_i	Shift values of the detected ridge lines

crack growth rates as measured via Thermoelastic Stress Analysis (TSA) along a unique slope at different stress ratios. In the work by Pitarresi and Cappello [21], an effective stress range ratio is measured from a fine analysis of the temperature signal in the vicinity of the closing crack; then, a value of the SIF is determined by the TSA of the crack tip. Both in the work by Pitarresi and Cappello [21] and Bercelli et al. [4], it is found that the conventional framework of TSA, which relies on the first harmonic of the temperature under cyclic loading, is not adapted to the case of closing cracks, for which higher-order harmonics should be considered. Indeed, discontinuities in the temperature signal are observed, due to the alternative crack opening and closing within one load cycle. This peculiar thermal signature is used in the work of Pitarresi and Cappello [21] to estimate an effective stress range. The present study aims to suggest a robust method to assess fatigue crack closure using infrared measurements. It should be noted that this paper solely addresses the influence of crack closure on the infrared measurements; no method for the assessment of the SIF with consideration of crack tip plasticity is addressed. The proposed method relies on an automated analysis of temperature signals via continuous wavelet transform. The exploration of the signal in a coherent time–frequency space allows for the estimation of crack closing and opening instants that are associated with high-frequency components. Then, the effective stress range ratio τ_o, as introduced by Elber [6], can be estimated. It must be noted that this method relies on full-field measurement (infrared thermography) and as such does not require prior knowledge of the position of the crack. In this context, this technique is not limited to conventional CT specimens, but is also suitable for the testing of structures (e.g. welded joints [4,22], WAAM rough surfaces [23]), thus allowing to consider the effects of local geometry and fabrication process.

This paper is divided in four sections. First, both the experimental and the numerical frameworks are presented; details on the loading configuration and test protocol are given, and steps to the creation of a thermomechanical simulation are given. The theoretical background of TSA is also briefly discussed. Second, linear elastic numerical simulation results are presented to illustrate the effect of crack closure on the temperature linked to the thermoelastic coupling. Explanations are provided as to why conventional first harmonic TSA is not suitable for the study of closing fatigue cracks. Third, the proposed methodology for the automatic assessment of the effective stress range ratio τ_o based on infrared measurements is presented. The method is then validated based on linear elastic numerical simulations. Finally, this methodology is applied to the experimental infrared data and results are discussed.

2. Test set-up and methods

The aim of the test is to detect and measure the crack closing for a crack of controlled length. The chosen material, sample geometry and test protocol to achieve this are described in this section.

2.1. Test set-up and equipment

The material of study is DH36 naval-grade steel (yield stress of 360 MPa). The thermomechanical parameters (density ρ, specific heat c, coefficient of thermal expansion α and conductivity λ) of this material, taken from the work by Carteron et al. [22], are given in Table 1.

In order to control the initiation site of fatigue cracks and their propagation in Mode I under cyclic loading, a notched sample was

Table 1
Thermomechanical parameters of DH36 steel, as taken from [22].

ρ(kg·m^{-3})	c(J.kg^{-1}·K^{-1})	α(K^{-1})	λ(W·m^{-1}·K^{-1})
7803	426	1.267×10^{-5}	47.1

designed, as illustrated in Fig. 1a. The sample is a 160 mm by 38 mm coupon, 6.5 mm thick, with a 3 mm diameter hole at its centre, on the periphery of which are two 0.25 mm diameter notches. The notches were obtained by wire electrical discharge machining. Tests were carried out using a hydraulic tensile testing machine with a 250 kN load capacity. The testing machine was force-controlled to ensure a constant amplitude sinusoidal loading at the chosen frequency. The sample was coated with a high-emissivity black paint to allow temperature field monitoring via the InfraTec ImageIR 10300 infrared camera (Fig. 1b). Four markers are drawn on the sample with low emissivity paint (Fig. 1b) to allow for motion compensation prior to any post-processing of infrared films.

To ensure the initiation and propagation of cracks at both notches in a reasonable time, the sample was loaded under cyclic tension for a load ratio of $R_{nom} = \frac{F_{min}}{F_{max}} = 0.1$ and at a load amplitude of $F_a = 20.25$ kN ($\sigma_a = 82$ MPa). Infrared films were recorded regularly to monitor cracks via Thermoelastic Stress Analysis (TSA). Once cracks of desired length l are detected at each notch, infrared films of 1000 frames at a sampling frequency f_c of 100 Hz are recorded for different mechanical frequencies f_m and multiple load ratios R_{nom} with a constant load amplitude of $F_a = 15.75$ kN ($\sigma_a = 64$ MPa). This loading magnitude is chosen in order to lower the SIF at the crack tip hence limiting the crack propagation during infrared film recording.

The infrared camera was set at an integration time of 2200 μs which is recommended for temperature ranges from −10 °C to 30 °C. Recorded infrared images have a resolution of 1536 × 1056 pixels, with a pixel size corresponding to roughly 40 μm.

In order to illustrate the applicability of the proposed crack closure assessment methodology for different experimental conditions, the combined effect of the crack length l, load ratio R_{nom}, and mechanical frequency f_m is explored. A total of 72 configurations are tested with:

- three crack lengths l of $1mm$, $3mm$ and $6mm$ (corresponding to respectively $\Delta K = 13.4MPa\sqrt{m}$, $\Delta K = 17.2MPa\sqrt{m}$ and $\Delta K = 23.2MPa\sqrt{m}$, as estimated via finite element analysis with linear elastic assumption);
- six load ratios R_{nom} of 0.1, −0.5, −1, −3, −6 and 10;
- four mechanical frequencies f_m of $1Hz$, $2Hz$, $5Hz$ and $10Hz$.

The three crack lengths l of 1, 3 and $6mm$ are chosen because they can be considered as small, medium and large, respectively, with regards to both the infrared camera resolution and conduction effects for typical metallic materials. The choice of the six load ratios R_{nom} between 10 and −6 allows the exploration of configurations from a fully open crack to a completely closed crack. The four mechanical frequencies f_m are chosen between 1 and $10Hz$, as they are common orders of magnitude when using hydraulic testing machines.

2.2. Thermoelastic stress analysis for the monitoring of surface fatigue cracks

TSA is a field measurement technique that allows the observation of gradients in the field of the first invariant of the stress tensor $I_1 = trace(\underline{\sigma})$. This makes it an effective *in-situ* method to detect and monitor surface fatigue cracks on structures under cyclic loading [4,22–25]. This section presents the theoretical background of TSA and a practical explanation of its application for the monitoring of fatigue cracks under different loading scenarios.

The method of TSA relies on the post-processing of the temperature measured at the surface of a structure under cyclic loading using an infrared camera. The temperature variation $\theta = T - T_0$ (with T the temperature of the material and T_0 its initial temperature) can be divided into two contributions:

- a progressive rise towards a stabilised mean temperature θ_d (under certain conditions) linked to the intrinsic dissipation Δ;
- an immediate temperature variation θ^a_{the} linked to the thermoelastic coupling C_{the}.

For the TSA technique, only the temperature variation θ^a_{the} linked to the thermoelastic coupling is of interest as it can be linked to the local stress amplitude. Indeed, the local heat equation gives

$$\rho c \frac{\partial \theta}{\partial t} = -div(\vec{q}) + C_{the} + \Delta \tag{1}$$

with $\vec{q}$ the local heat flux. In the case of small temperature variations (*i.e.* $\frac{\theta}{T_0} \ll 1$), the thermoelastic coupling heat source C_{the} is [26]

$$C_{the} = -T_0 \alpha \left(\frac{\partial I_1}{\partial t} + \alpha \frac{\partial \theta}{\partial t} \frac{3E}{1-2\nu} \right) \tag{2}$$

where E is the Young modulus and ν the Poisson coefficient. Moreover,

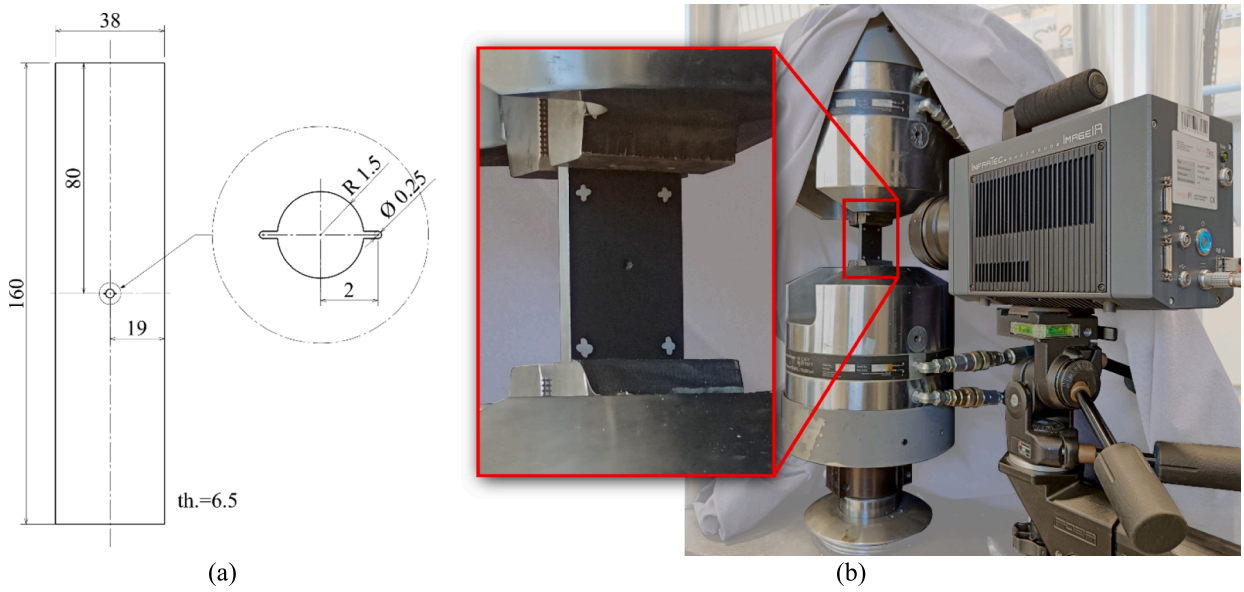

Fig. 1. Sample dimensions in millimetres (a) and view of the sample mounted in the test machine and monitored with an infrared camera (b).

for classical steel materials at room temperature, it is found that $\alpha^2 \frac{3E}{1-2\nu} T_0 \ll \rho c$. In this context, for an isotropic material under adiabatic conditions, the local heat equation gives

$$\frac{\partial \theta^a_{the}}{\partial t} = -\frac{\alpha T_0}{\rho c} \frac{\partial I_1}{\partial t} \tag{3}$$

where θ^a_{the} is the temperature variation linked to the thermoelastic coupling under adiabatic conditions. As a result, the local value of θ^a_{the} through time can be used to estimate the corresponding stress I_1. For instance, considering the case of a fully linear elastic structure subjected to a sine loading of frequency f_m, the magnitude of the component at frequency f_m of the temperature linked to the thermoelastic coupling θ^a_{the} (*i.e.* the amplitude of the first harmonic, noted θ^a_1) is proportional to the amplitude of the first invariant of the stress tensor I_{1_a} as follows

$$\theta^a_1 = \frac{\alpha T_0}{\rho c} I_{1_a}. \tag{4}$$

It should be noted that, given the negative sign in equation (3), the temperature signal θ^a_{the} and the stress signal I_1 are in opposite phase. In other words, when the material is in tension, its temperature decreases, and when the material is in compression, its temperature rises.

2.3. Thermomechanical finite element simulation

Two configurations are considered:

- a simple 2D crack centred in a large plate (Fig. 2a), which goal is to explore and illustrate the effect of the temperature signal on the closing of the crack (see §3);
- the test configuration (Fig. 2b) in 2D, which goal is to demonstrate the applicability of the proposed methodology for crack closure assessment and validate its results (see §4.3).

Simulations are conducted in two consecutive steps:

- the first step is a linear elastic mechanical calculation to evaluate the thermoelastic heat source term C_{the} during one loading cycle, from the knowledge of the field of I_1 (equation (2));
- the second step is a thermal calculation, which uses the previously determined thermoelastic heat source C_{the} as input and gives the corresponding temperature variations considering conduction effects as output.

Both configurations are considered as 2D plane stress, and advantage is taken of symmetries to reduce computation costs. Geometries are quad-meshed with biquadratic elements (CPS8 in Abaqus) as illustrated in Fig. 2. Except for a dense mesh, no particular care was taken to address the crack tip singularity, and the model is considered fully elastic.

- for the simple centred crack configuration (Fig. 2a), the crack is modelled as an Abaqus crack seam and self-contact is introduced to allow crack closure under compressive stress;
- for the test sample geometry (Fig. 2b), the crack is modelled as a free edge of length l in frictionless contact with a fully rigid component to allow crack closure under compressive stress.

For both configurations, the mechanical simulation step consists in the application of a nominal stress σ_{nom} at the upper edge of the geometry. Only one load cycle is simulated, for which the nominal stress at increment i is defined as

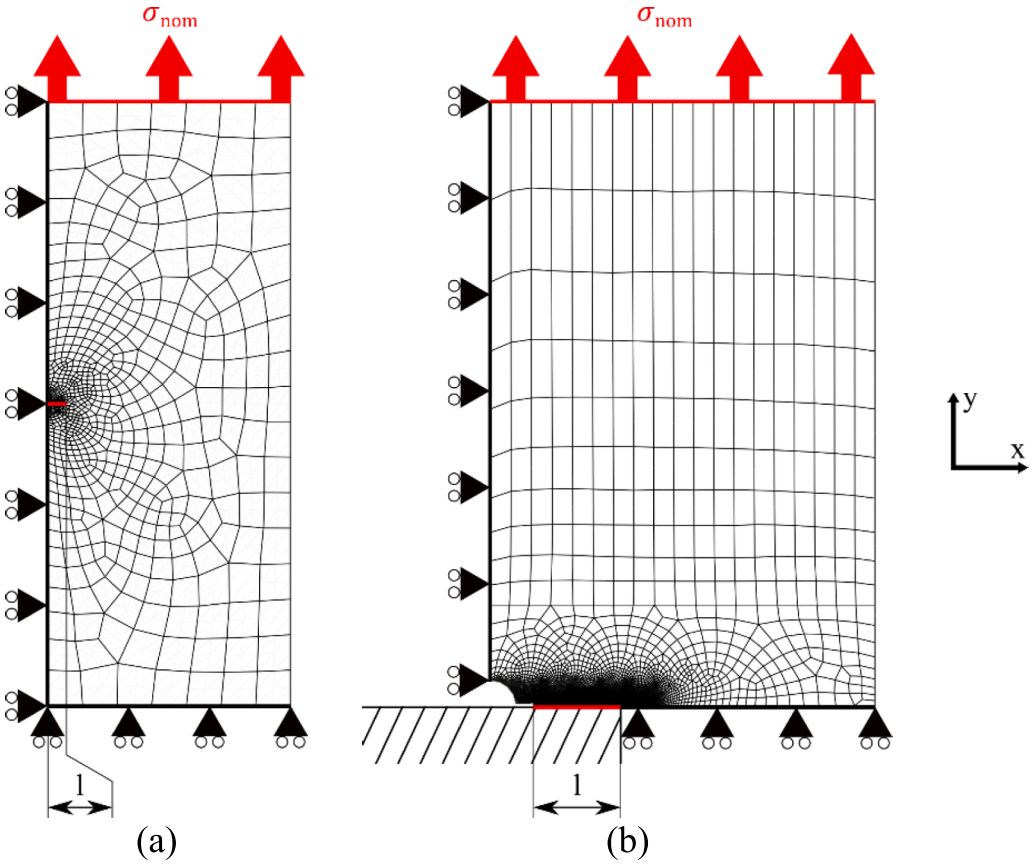

Fig. 2. Mesh detail for the FE simulations of a 2D crack in the middle of a large plate (a) and at the notch of the test sample geometry (b).

$$\sigma_{nom}(i) = \frac{\Delta\sigma_{nom}}{2}\sin(2\pi f_m i\Delta t) + \frac{1 - R_{nom}}{1 + R_{nom}}\sigma_a^{nom} \tag{5}$$

where σ_a^{nom} is the nominal stress amplitude and Δt is the time step which is chosen to be equal to 0.005 s.

For the thermal simulation step, the exact same meshing as the mechanical simulation is used, except that the elements are changed to heat transfer elements (DC2D8 in Abaqus). Multiple loading cycles are simulated to allow for heat transfer equilibrium. In this context, thermal simulations of a 6*s* duration with a step time Δt of 0.005 s are computed (twenty times the minimum mechanical period). The post-processing of the numerical results presented in the following is performed in a time range between 2 and 6 s as satisfactory stabilisation is observed at 2 s. It must be noted that such a choice of time range induces post-processing over a different number of loading cycles depending on the loading frequency f_m; this is consistent with the experimental approach for which the infrared film duration remains constant for all loading conditions. Similarly, the post-processing of the numerical results is performed using a sampling frequency of $f_c = 100$ Hz, as in real experimental conditions.

This proposed numerical framework allows for a preliminary study, analysing the influence of crack closing on the temperature linked to thermoelastic coupling (cf. §3), and for the validation of the method of crack closing assessment in a perfectly elastic case (cf. §4.3).

3. Crack closure influence on temperature linked to thermoelastic coupling

TSA, as a mechanical field measurement technique, allows for the *in-situ* observation of stress risers such as surface cracks. This paragraph addresses practical methods for crack detection under different loading types, namely repeated tension and tension–compression in Mode I. Results illustrated in this paragraph are obtained from the numerical simulation of a 2D through crack in a large plate (Fig. 2a) in linear elasticity.

It is important to note that two phenomena can alter the nature of the temperature signal close to a crack under cyclic loading, namely dissipation linked to crack tip plasticity and stress reversals linked to crack closure. The present study focuses on the latter (crack closure) and therefore all numerical simulations presented below are conducted in linear elasticity.

3.1. Cracks in repeated tension in Mode I

The principle of TSA applied to the 2D case of a 3 mm long through crack in a DH36 plate submitted to a sine cyclic tension of stress amplitude $\sigma_a^{nom} = 200$ MPa, load ratio $R_{nom} = 0$ and mechanical frequency $f_m = 10$ Hz and 2 Hz is presented in this section. Simulation results from the simple centred crack configuration (Fig. 2a) considering

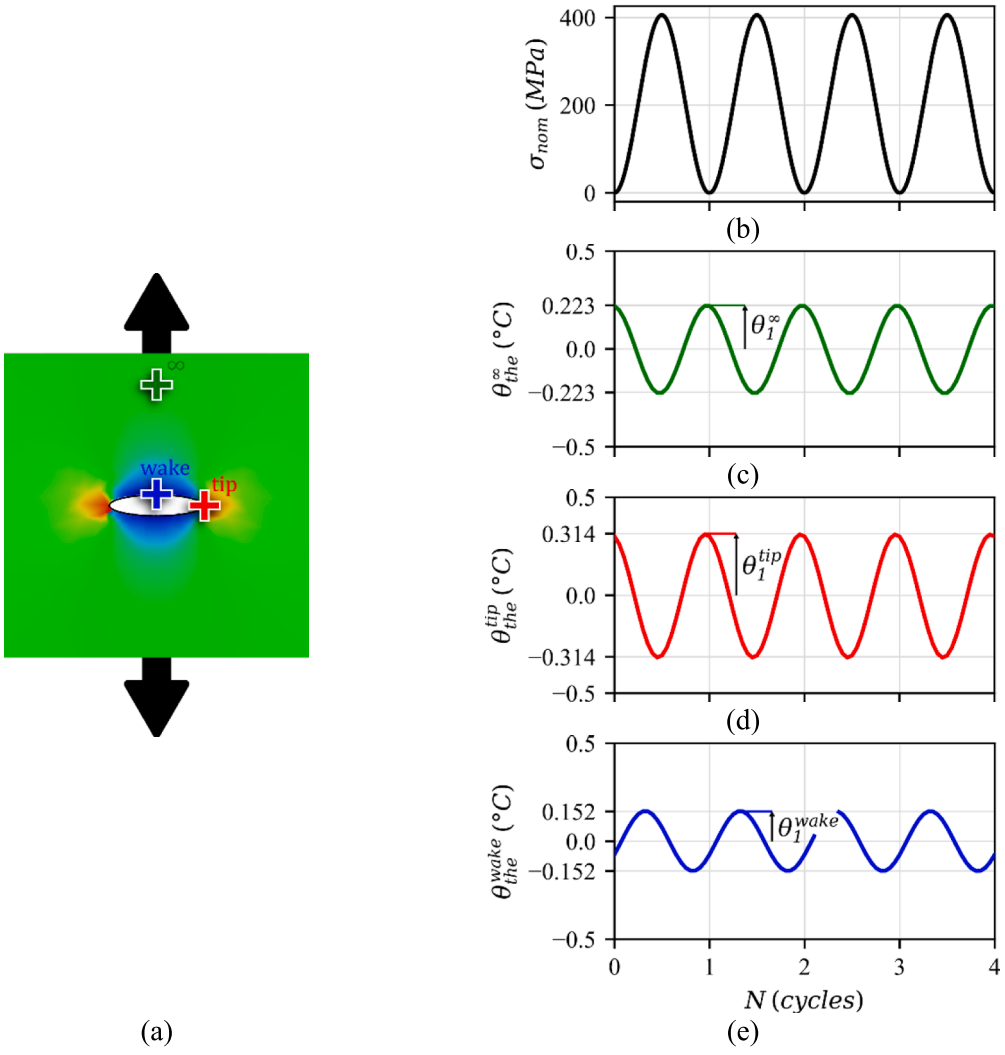

Fig. 3. Illustration of the field of I_1 around a 2D through crack in Mode I at $R = 0$ (a), nominal stress signal (b), corresponding thermal signals far from the crack (c), at the crack tip (d) and at the crack wake (e) for $f_m = 10$ Hz.

conduction effects are used to illustrate this case (see §2.3 for details on the simulation process). It must be noted the following results are based on a fully elastic simulation.

An illustration of the field of I_1 at the maximum load is given in Fig. 3a; the crack (in Mode I) is fully open and stress concentrations exist at both crack tips whereas lower stress is found at the crack wake. As the specimen is loaded under cyclic tension ($R_{nom} \in [0:1[$), the crack is always open during a loading cycle. Hence, as it can be observed from thermal signals (Fig. 3b, c and d), a sine nominal loading leads to a sine thermoelastic response near the crack. The temperature signal at position (x,y) on the 2D plate can then be described as

$$\theta_{the}(t,x,y) = \theta_1(x,y)\sin(2\pi f_m t + \phi_1(x,y)) \tag{6}$$

where ϕ_1 is the phase shift of the signal due to thermal conduction. The amplitude of the first harmonic θ_1 of the temperature signal linked to the thermoelastic coupling is highest at the crack tip (due to stress concentration) and lowest at the crack wake (as there are free edges). Noting θ_1^{∞} the first harmonic amplitude of the temperature far from the crack, θ_1^{tip} the first harmonic amplitude at the crack tip and θ_1^{lip} the first harmonic amplitude at the crack wake, it is observed that

$$\theta_1^{tip} > \theta_1^{\infty} > \theta_1^{wake} \tag{7}$$

In such a case, the estimation of the field of the temperature's first harmonic amplitude θ_1 from the infrared data allows the observation of a surface crack (owing to its peculiar heterogeneous stress field) and the estimation of its length via image processing [22,23,27]. In practice, a fast and efficient method for the estimation of the field of θ_1 is the lock-in method [28]; it is applied to the numerical simulation data below. The results are illustrated in Fig. 4 where both the maps of θ_1 and ϕ_1 are plotted for two mechanical frequencies of 10 Hz and 2 Hz. The position and length of the observed crack are indicated by black solid line.

It is important to note here the influence of the mechanical frequency f_m on the detectability of the crack: the higher the mechanical frequency, the lesser the conduction and so the higher the gradients in θ_1 (*cf.* Fig. 4a and b). The increase of f_m by a factor of 2 has the same effect as reducing the conductivity λ by half. In practice, when performing conventional TSA, the highest achievable mechanical frequency is preferable (while limiting temperature rise to avoid material behaviour alteration). The influence of f_m is also visible on the phase parameter ϕ_1 (Fig. 4c and d): stronger and broader delay effects exist with higher conduction, hence the results in the field of ϕ_1. The phase can then be an interesting indicator for materials with strong conductivity or for tests with low mechanical frequency [29–31].

3.2. Cracks in tension–compression in Mode I

The principle of TSA applied to the 2D case of a 3 mm long through crack in a DH36 plate loaded in cyclic tension at a stress amplitude $\sigma_a^{nom} = 200$ MPa, load ratio $R_{nom} = -3$ and mechanical frequency $f_m = 10$ Hz, is presented in this section. Simulation results from the simple centred crack configuration (Fig. 2a) considering conduction effects are used to illustrate this case (see §2.3 for details on the simulation process). It must be noted that the following results are based on a fully elastic simulation. Fig. 5a illustrates the field of I_1 at both maximum and minimum load. The crack (in Mode I) is alternately closed and opened depending on the sign of the nominal loading ($R_{nom} < 0$). As a result, contrary to what was observed in §3.1 for $R_{nom} \in [0:1[$, a sine nominal loading no longer leads to sine temperature signal (Fig. 5b, c and d). Indeed, the temperature signal linked to the thermoelastic coupling at

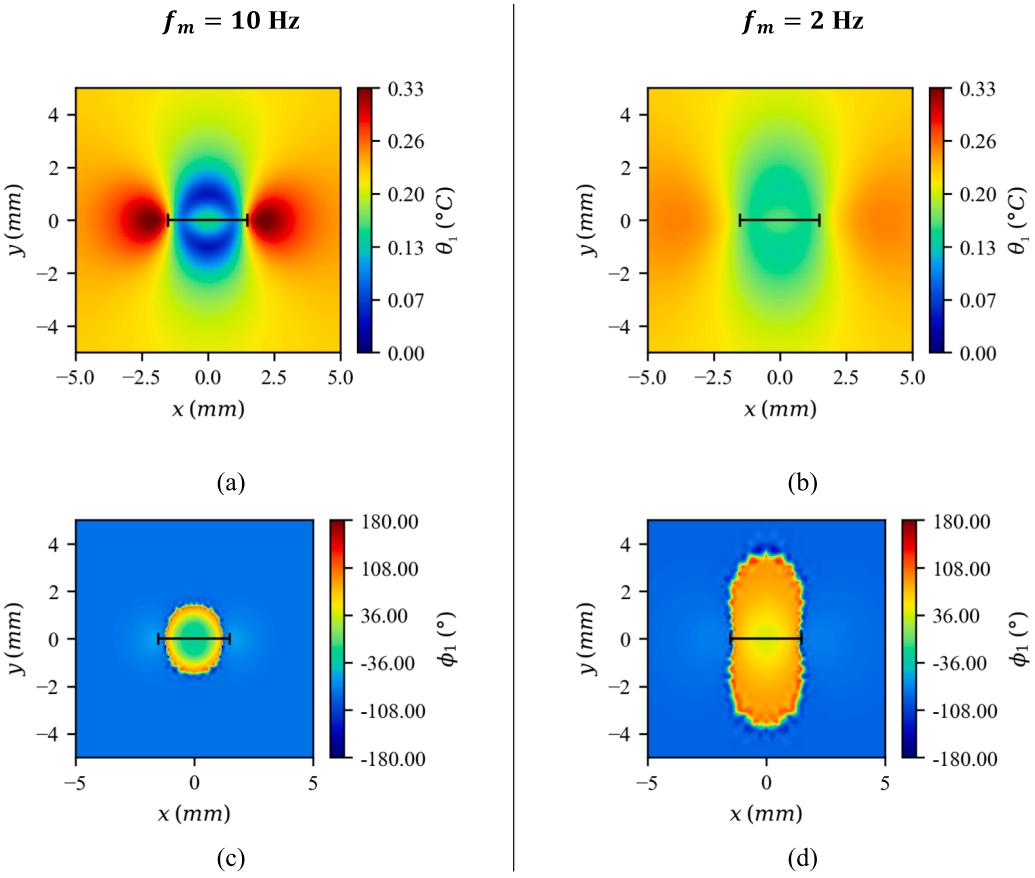

Fig. 4. Map of numerical values of the temperature's first harmonic amplitude θ_1 at $f_m = 10$ Hz (a), at $f_m = 2$ Hz (b), and phase ϕ_1 at $f_m = 10$ Hz (c) and at $f_m = 2$ Hz (d) for $R = 0$.

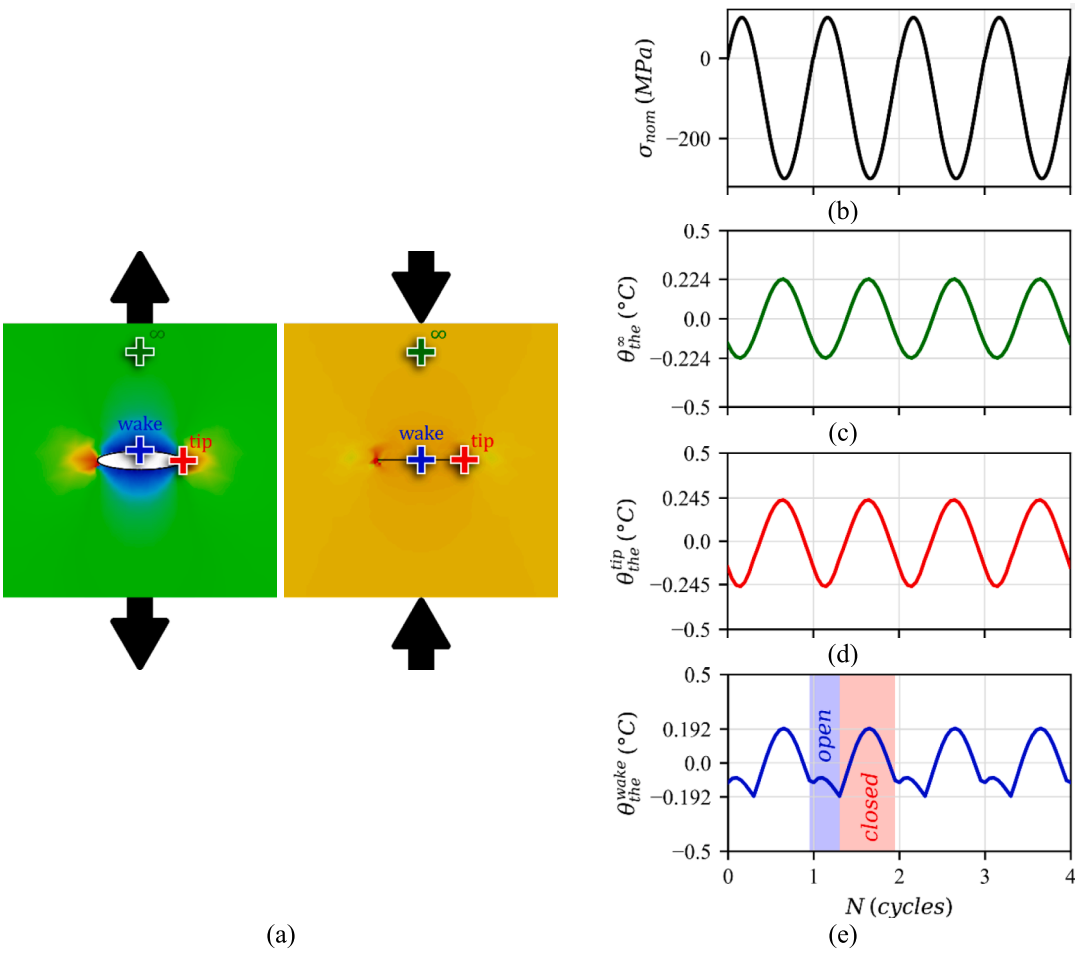

Fig. 5. Illustration of the field of I_1 around a 2D through crack in Mode I at $R = -3$ both open and closed (a), nominal stress signal (b), corresponding thermal signals far from the crack (c), at the crack tip (d) and at the crack wake (e).

the wake of the crack (Fig. 5d) displays a very peculiar evolution, corresponding to the alternance between the closure and opening of the crack. In this context, the temperature's first harmonic amplitude θ_1 is no longer an adapted indicator of the presence of a crack. The second harmonic amplitude θ_2 (at the frequency $2 \times f_m$) is preferred here, because its field highlights the wake of the closing crack, allowing for its detection and length estimation. It should be noted that in practice, the presence of plasticity is also responsible for higher-order components at the crack tip [32]. Such effect is not depicted in the following numerical results, because simulations are conducted in linear elasticity.

Numerical maps of the first harmonic amplitude θ_1 and second harmonic amplitude θ_2 for $R_{nom} = -3$ and $f_m = 10$ Hz computed via lock-in are shown in Fig. 6a and b, respectively. Compared to the case at $R_{nom} = 0$ (Fig. 4), the crack is hardly visible in the map of θ_1 at $R_{nom} = -3$, as could be expected from the signals shown in Fig. 5. It is however visible in the map of θ_2. However, the reader's attention is drawn to the values of θ_2, ranging from 0 °C to approximately 0.05 °C. The detection of such small temperature variations relies on good experimental practice. First, the mechanical frequency must be maximised to ensure high-magnitude temperature signals and to limit conduction, as illustrated in §3.1.

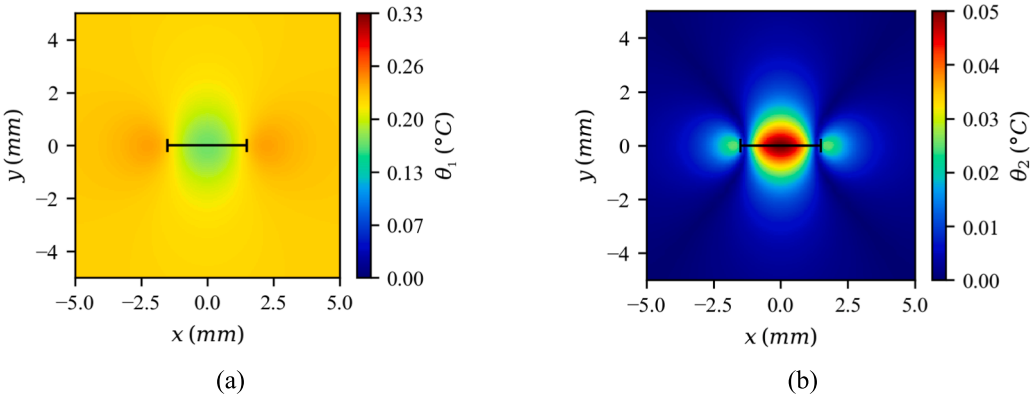

Fig. 6. Map of numerical values of the temperature's first harmonic amplitude θ_1 (a) and second harmonic amplitude (b) for $R_{nom} = -3$ at $f_m = 10$ Hz.

Second, a high-resolution infrared camera, with an adapted integration time (to limit noise) and a high acquisition frequency, is required.

4. Method for assessment of the crack closure and numerical validation

As shown via numerical simulations (§3.2), the presence of a crack closure phenomenon affects the temperature response θ_{the} close to the crack. Further processing of this temperature signal allows for the measurement of the crack opening time during one loading cycle. From this opening time, it is possible to calculate an effective stress range ratio τ_o, *i.e.* the ratio of the effective stress range $\Delta\sigma_{eff}$ (stress range that drives the crack propagation) and the nominal stress range $\Delta\sigma_{nom}$, defined as

$$\Delta\sigma_{eff} = \tau_o \Delta\sigma_{nom} \tag{8}$$

A method to measure τ_o from infrared data is detailed in the present section. It is then validated using linear elastic thermomechanical simulations.

4.1. Effective stress range ratio

In order to give an expression of the effective stress range ratio τ_o, the case of a perfectly linear elastic plate with a 2D through crack loaded in Mode I under tension–compression ($R_{nom} < 0$) is considered: the crack is fully open when the nominal stress σ_{nom} is positive (tension), and the crack is fully closed when the nominal stress σ_{nom} is negative (compression). It is assumed that the crack can only propagate when it is open, *i.e.* when σ_{nom} is positive. In such conditions, the effective stress range $\Delta\sigma_{eff}$ corresponds to the portion of loading in tension, and is thus equal to the maximal nominal stress σ_{max} (Fig. 7).

As shown in §3.2, the temperature at the closing crack wake θ_{the}^{wake} shows discontinuities that account for the transition from the opened state to the closed state of the crack, and vice versa (Fig. 7). The instant of opening at cycle n is noted o_n, and the consecutive closing time is noted c_n. The time of crack opening within one loading cycle $t_o = |c_n - o_n|$ can then be estimated via signal processing of θ_{the} as measured by an infrared camera.

For a sine nominal load of frequency f_m, one can then determine the value of the effective stress range ratio τ_o from infrared measurement using the following relation

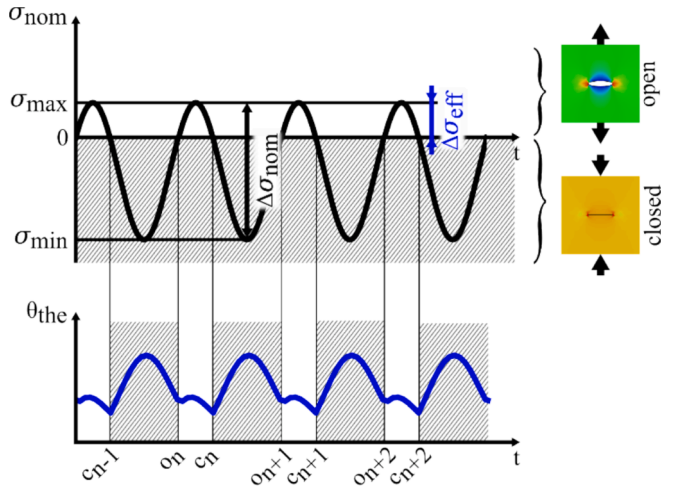

Fig. 7. Schematic representation of the nominal stress range $\Delta\sigma_{nom}$ and effective stress range $\Delta\sigma_{nom}$ on the nominal loading signal σ_{nom} for a loading ratio $R_{nom} < 0$ and corresponding temperature response at the crack wake (imposing a zero phase) with indications of consecutive times of crack closing c_n and opening o_n at cycle n.

$$\Delta\sigma_{eff} = \tau_o \Delta\sigma_{nom} = \frac{1 - \cos(\pi f_m t_o)}{2} \Delta\sigma_{nom} \tag{9}$$

4.2. Proposed methodology for the assessment of the effective stress range ratio

The assessment of the effective stress range $\Delta\sigma_{eff}$ solely from infrared data requires the definition of a robust temperature signal processing method. The method proposed in this paper relies on the analysis of the scalogram of a signal, namely the value of its Continuous Wavelet Transform (CWT) coefficients as a function of time and frequency (or scale). Indeed, the opening and closing of a crack give rise to discontinuities at times o_n and c_n (Fig. 7) in the temperature signal, which can be associated with high-frequency components.

The aim of the algorithm is to provide the user with, as output, the opening rate field $\tau_o(P_i)$ at pixel P_i given, as input, an infrared film. The method relies on five user parameters:

- the standard deviation ϵ_{IR} of the noise of the infrared temperature estimation;
- the significant level of temperature variation θ_1^{th};
- the number of harmonics n_h for signal reconstruction via Discrete Cosine Transform (DCT);
- the sampling frequency f_{DCT} for signal reconstruction via DCT.
- the phase value ϕ_{ref} of the temperature's first harmonic at a reference position (*i.e.* position in the structure of interest where no crack exists)

First, the temperature variation at pixel P_i is taken from the infrared film of n_P pixels. To determine if crack closing and opening phenomena exist at pixel P_i, a comparison is made between the standard deviation SD of the temperature at P_i, processed via a high pass filter of cut-off frequency $2 \times f_m$, noted $\theta_{2\hat{f}_m}(P_i)$, and the noise standard deviation ϵ_{IR}

$$\mathrm{SD}(\theta_{2\hat{f}_m}(P_i)) > \epsilon_{IR} \tag{10}$$

This criterion ensures the existence of significant components, with respect to experimental noise, at frequencies higher than those of the first harmonic (mechanical frequency f_m). Indeed, such higher frequency components can be attributed to the alternative opening of a crack within one loading cycle.

If the standard deviation criterion is not met (*i.e.* absence of significant high frequency components), the amplitude of the first harmonic $\theta_1(P_i)$ is compared to the threshold value θ_1^{th}. If $\theta_1(P_i) > \theta_1^{th}$, a non-negligible stress magnitude (in the sense of I_1) exists at P_i resulting in $\tau_o = 0$ (*i.e.* no crack or fully closed crack). On the contrary, if $\theta_1(P_i) \leq \theta_1^{th}$, the stress at P_i is considered negligible and $\tau_o = 1$ (*i.e.* fully opened crack or P_i outside the surface of observation).

If the standard-deviation criterion is met (*i.e.* presence of significant high frequency components), the effective stress range ratio τ_o measurement technique based on CWT is applied. The temperature variation $\theta_{the}(P_i)$ is first reconstructed via DCT. The reconstructed signal $\theta_{the}^{DCT}(P_i)$ is characterised by both limited noise, given an appropriate number of harmonics n_h, and increased temporal resolution, with sampling frequency $f_{DCT} > f_c$,

$$\theta_{the}^{DCT}(P_i, j) = \sum_{k=0}^{n_h} \theta_k(P_i) \cos\left(2k\pi f_m \frac{j}{f_{DCT}} + \phi_k(P_i) + \frac{\pi}{2}\right) \tag{11}$$

A Ricker type wavelet ("mexican hat") $\Psi_{a,b}$ is chosen to perform the CWT of $\theta_{the}^{DCT}(P_i)$, of scale a and shift b,

$$\Psi_{a,b}(t) = \frac{2}{\sqrt{3a}\pi^{\frac{1}{4}}} \left(1 - \left(\frac{t-b}{a}\right)^2\right) e^{\left(\frac{t-b}{\sqrt{2}a}\right)^2} \tag{12}$$

The Ricker wavelet is characterised by an apparent frequency $f_{app} = \frac{1}{2\sqrt{3}a}$. Approximately 98 % of the wavelet energy is found in a time window of length $2\pi a$.

The CWT approach consists in the computation of the scalogram s_{CWT} of the signal $-\theta_{the}^{DCT}(P_i)$, *i.e.* the result of its convolution with the chosen wavelet $\Psi_{a,b}$ in the (a,b) plane

$$s_{CWT}(P_i,a,b) = -\int_{-\infty}^{+\infty} \theta_{the}^{DCT}(P_i,t) \times \Psi_{a,b}(t)\mathrm{d}t \tag{13}$$

The CWT of a signal allows for its coherent representation in both the time and frequency domains: the 2D plot of $s_{CWT}(a,b)$ gives an image of the evolution of the signal's frequency (or inverse of the scale a) in time (or shift b). In order to analyse the temporal evolutions of core frequencies of the reconstructed signal $\theta_{the}^{DCT}(P_i)$, the scales a are defined from $\frac{1}{2\sqrt{3}n_h f_m}$ to $\frac{1}{2\sqrt{3}f_m}$ with a resolution of $\frac{1}{f_{DCT}}$. To avoid edge effects related to the CWT convolution and because the signal of interest is periodic, $\theta_{the}^{DCT}(P_i,j)$ is defined for j from 0 to $\left\lfloor \frac{(2\pi+\sqrt{3})f_{DCT}}{\sqrt{3}f_m} \right\rfloor$ and $\Psi_{a,b}$ is limited for b over one cycle, from $\frac{\pi}{\sqrt{3}f_m}$ to $\frac{\pi+\sqrt{3}}{\sqrt{3}f_m}$. The presence of signal singularities at higher frequencies (or lower scales a) supposedly corresponds to the opening and closing instants at cycle n, respectively o_n and c_n. The detection of signal singularities is performed by definition of n_{RL} ridge lines in the scalogram s_{CWT} of $-\theta_{the}^{DCT}$, according to the algorithm proposed by Du et al. [33]. If more than two ridge lines ($n_{RL} \geq 2$) are found, the shifts b_1 and b_2 at the lowest scale $a = \frac{1}{2\sqrt{3}n_h f_m}$ (highest frequency) of the two longest ridge lines are assumed to be, indifferently, consecutive instants of closing and opening of the crack [21]. At this point, it is not known whether the measured time $|b_1 - b_2|$ corresponds to the closing time or the opening time of the crack. To solve this ambiguity, a reference phase value ϕ_{ref} (measured from a reference position chosen by the user) is used, a parameter p is determined

$$p = \left\lfloor \frac{2\pi \max(b_1,b_2) f_m + \phi_{ref}}{\pi} \right\rfloor \quad \text{and}$$
$$\begin{cases} \text{if } p \text{ even(loading) then } t_o = |b_1 - b_2| \\ \text{if } p \text{ odd (unloading) then } t_o = \frac{1}{f_m} - |b_1 - b_2| \end{cases} \tag{14}$$

It is worth noting that, due to higher compressive stress as observed in Fig. 8, a higher temperature rise near the crack is expected during closing than during opening. However, it is not necessarily the case in practice. This was indeed observed specifically on some numerical cases (e.g. $a = 6mm$ and $R_{nom} = -0.5$ for which there is little crack closing) due to conduction effects, depending on the mechanical frequency f_m and the position along the crack wake, the temperature rise would be higher during the opening than during the closing of the crack. As a result, the definition of a reference position and the corresponding reference phase ϕ_{ref} appears essential to unambiguously compute the opening time t_o from the measured instants b_1 and b_2.

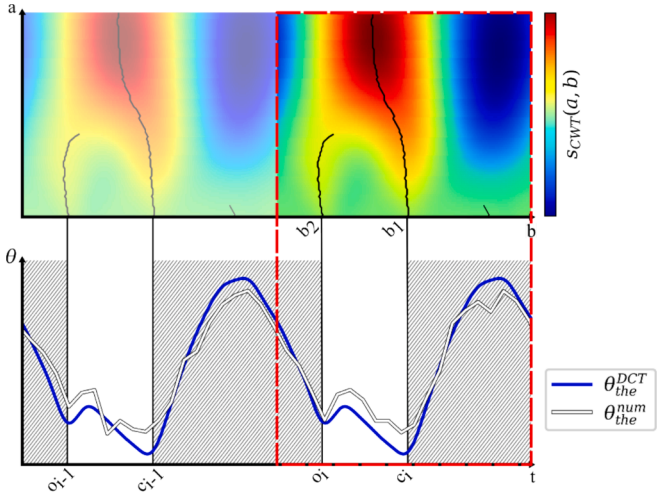

Fig. 8. Illustration of the CWT method for the opening rate measurement.

Then, the opening rate can be computed $\tau_o(P_i) = \frac{1-\cos(\pi f_m t_o)}{2}$. This process is illustrated in Fig. 8 for a numerical temperature θ_{the}^{num} taken at the centre of a $3mm$ long crack under a sine load of amplitude $F_a = 35kN$, frequency $f_m = 5Hz$ and load ratio $R_{nom} = -3$, with an added Gaussian noise of $30mK$ standard deviation and a sampling rate $f_c = 100Hz$. The figure shows the raw temperature signal θ_{the}^{num} and its DCT reconstruction θ_{the}^{DCT} in the lower graph, and the corresponding scalogram $s_{CWT}(a,b)$ in the upper graph. The red window shows the post-processed time range $\left[\frac{\pi}{\sqrt{3}f_m} : \frac{\pi+\sqrt{3}}{\sqrt{3}f_m}\right]$ free from convolution edge effects in which three ridge lines are found. A satisfactory estimation of the opening rate is found: $\tau_o = 0.27$; it is indeed close to the expected theoretical value $\tau_o^{th} = \frac{1}{1-R_{nom}} = 0.25$ for $R_{nom} = -3$.

If less than two ridge lines are found ($n_{RL} < 2$), then it is assumed that no alternative opening crack exists at pixel P_i, and the opening rate is determined according to the significant temperature variation magnitude criterion of threshold θ_1^{th}.

When all n_P pixels have been computed, the map of τ_o is provided to the user as output. The algorithm workflow is illustrated in Fig. 9.

4.3. Application of the methodology to numerical simulations results

The algorithm detailed in §4.2 is applied to thermomechanical simulations results. As numerical simulations are supposedly perfect (absence of experimental noise), they are used to prove the applicability of the method to effectively measure a field of the effective stress range ratio at different load ratios R_{nom}, mechanical frequencies f_m, and crack lengths l (see §2.1). As there is virtually no noise, ϵ_{IR} is set to $1mK$. The significant temperature amplitude θ_1^{th} is set to $57mK$, which corresponds to 80% of the θ_1^s value at nominal stress $\sigma_a^{nom} = \frac{F_a}{S}$ (see Eq. (4). As for DCT reconstruction, it was chosen $n_h = 10$ and $f_{DCT} = 10 \times f_c$.

For all 72 configurations, the complete numerical effective stress range ratio τ_o^{num} field around the notch is computed; each map is divided into four quarters to exhibit the effect of the four considered mechanical frequencies f_m. Since the numerical simulation is perfectly elastic, the effective stress range ratio τ_o^{num} is homogeneous along the crack wake, conduction effects put aside, meaning that the crack is either completely open or completely closed. This is the assumption made by Elber in his approach [6], where a SIF threshold K_{op} is defined. Nevertheless, the τ_o^{num} field is altered by the crack tip singularity. It is reminded that no particular care was taken to model the crack tip singularity. In this regard, the values of τ_o^{num} near the crack tip in Fig. 10 should not be considered.The temperature signal at the centre of the crack (at $l/2$, as indicated by a white cross in Fig. 10) during the last two loading cycles of the numerical simulation are plotted in Fig. 11 for all 72 loading configurations. The corresponding values of the effective stress range ratio are compared with the theoretical effective stress range ratio $\tau_o^{th} = \frac{1}{1-R_{nom}}$ for a linear elastic case.

For the short crack ($l = 1mm$, Fig. 12a), some differences to the theoretical tendency τ_o^{th} are observed, especially for $R_{nom} = 0.1$, $R_{nom} = -0.5$ and $R_{nom} = -1$. This is attributed to conduction effects that are particularly noticeable given the short length of the crack. Indeed, for a characteristic length of $1mm$ and given the material properties, the Fourier number $\mathscr{F}$ is equal to 5.7 at $f_m = 10Hz$, meaning that temperature gradients of about $1mm$ are very likely to be smoothed by

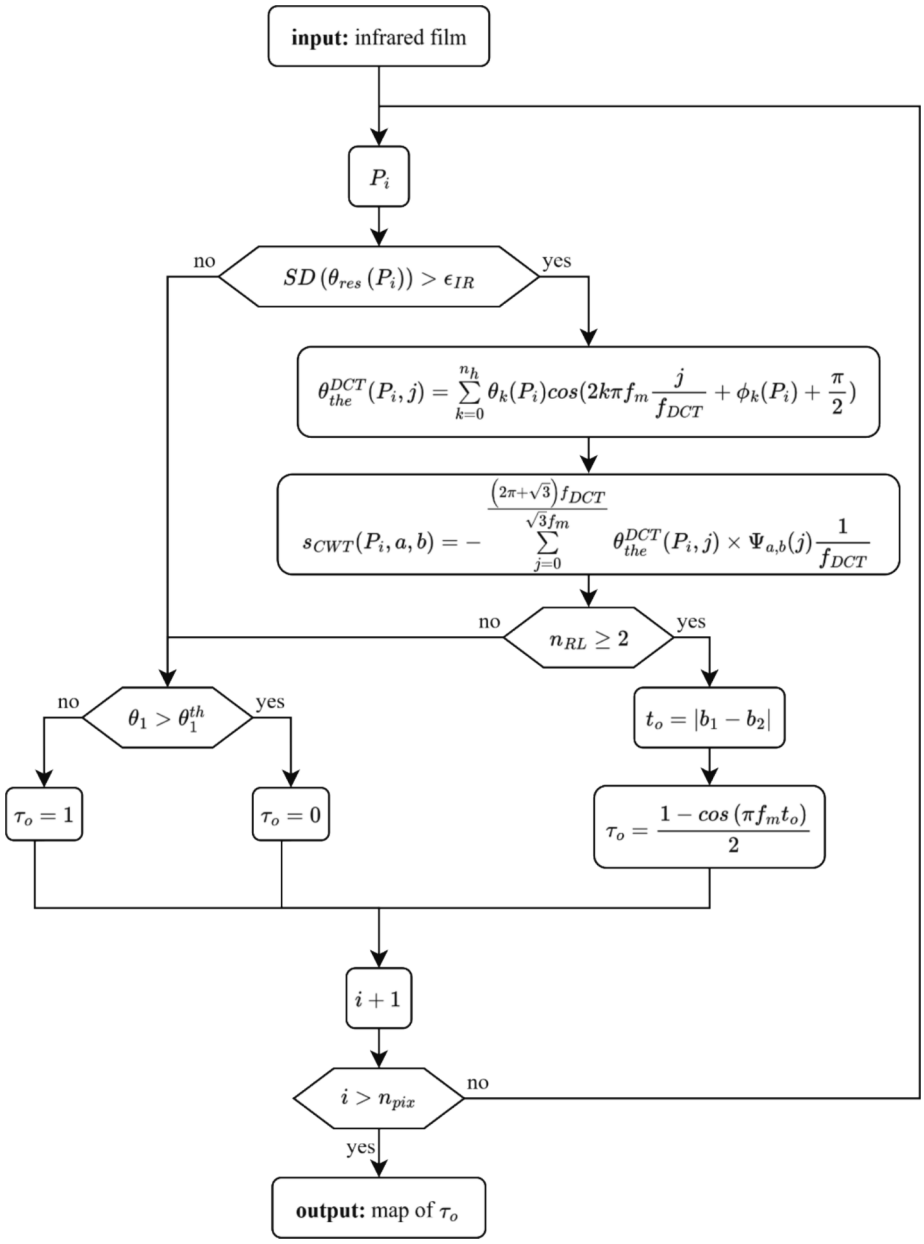

Fig. 9. Workflow of the opening rate τ_o measurement algorithm.

conduction effects (*i.e.* $\mathscr{F} \gg 1$). In that regard, the results found for $l = 1mm$ appear acceptable.

For the medium crack ($l = 3mm$, Fig. 12b), a quasi-perfect match is found for all values of load ratio R_{nom} and mechanical frequency f_m. Indeed, for such a characteristic length, the Fourier number at $f_m = 10Hz$ is equal to 0.6, meaning that the conduction effect should still allow for the detection of the crack via TSA (*i.e.* $\mathscr{F} \ll 1$).

For the long crack ($l = 6mm$, Fig. 12c), the results are satisfactory, except for the case at $R_{nom} = 0.1$ and $f_m = 10Hz$. This result is attributed to substantial longitudinal stress along the crack wake under Mode I, as the crack length is not negligible with respect to the sample dimensions. The temperature magnitude associated with such stresses is even more pronounced at high frequencies, for which conduction effects are limited, leading to the condition $\theta_1 > \theta_1^{th}$ (see Fig. 9), hence the erroneous value specifically at $f_m = 10Hz$.

Overall, the estimation of an effective stress range ratio τ_o^{num} field via the proposed methodology appears satisfactory when considering data from perfectly elastic thermomechanical simulations, except for the very specific cases of quasi fully open small cracks at low frequency and structurally long cracks.

5. Application of the methodology to experimental data

In this section, the algorithm detailed in §4.2 is used on experimental infrared data acquired for the 72 loading configurations (see §2.1) in order to demonstrate the applicability of the crack closure assessment method. Results are then discussed and limitations to the method are addressed.

5.1. Results

Non-negligible noise exists in the infrared data, which mostly depends on the camera and the choice of its integration time with respect to the temperature magnitude of the observed object. In this case, the integration time was set to $2200\mu s$, and the temperature of the sample varied between approximately $27^{\circ}C$ and $30^{\circ}C$. In such a configuration,

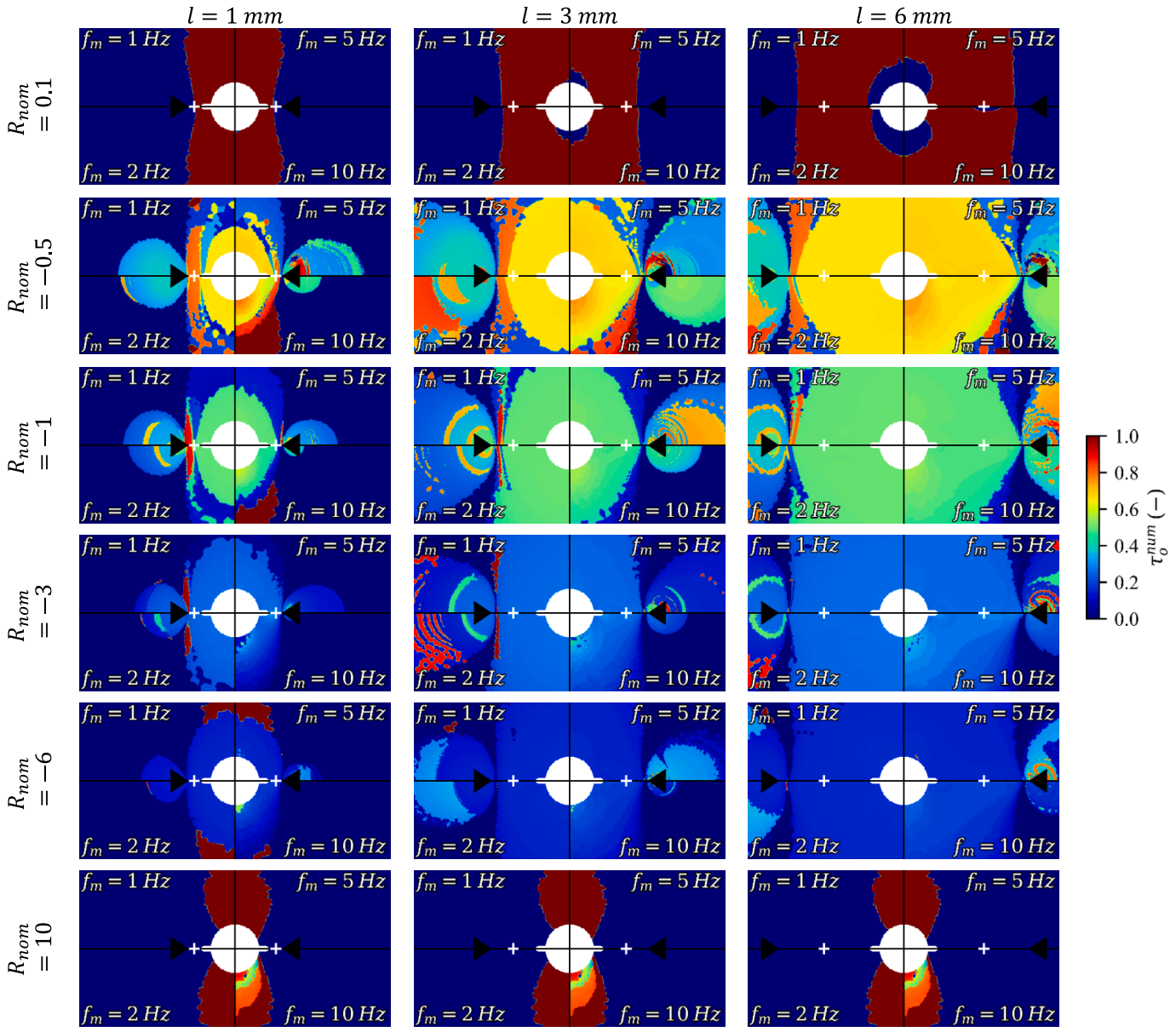

Fig. 10. Maps of the numerical effective stress range ratio τ_o^{num} around the central notch for different load ratios R_{nom}, mechanical crack lengths l; each map is divided in four quarters to represent the τ_o field depending on the mechanical frequency f_m; the tip of the crack is indicated by a black triangle.

based on prior analysis on a black body, the temperature noise standard deviation was estimated to approximately $25mK$. Prior to use of the effective stress range ratio measurement algorithm, a binning of infrared films of 5×5 is performed, both for the sake of computation time and experimental noise reduction. The noise standard deviation is then $\epsilon_{IR} = \frac{25}{\sqrt{5}} \approx 11mK$, for a pixel size of roughly $200\mu m$. The significant temperature amplitude θ_1^{th} is set to $51mK$, which corresponds to 80% of the θ_1^a value at nominal stress $\sigma_a^{nom} = \frac{F_a}{S}$ (see Eq. (4) considering the black paint emissivity (estimated at 0.9). As for DCT reconstruction, n_h is set at 10 and $f_{DCT} = 10 \times f_c$.

For the sake of readability and to facilitate the comparison of results for the 72 loading conditions, quarters of the measured τ_o^{exp} fields are illustrated in Fig. 13 (each quarter corresponding to a different loading frequency f_m). It appears that heterogeneous fields of τ_o^{exp} are measured along the crack wake. Despite noisy pixels, these fields are rather continuous around the crack. The heterogeneity of the τ_o^{exp} field, which was not observed in the numerical simulations, is attributed to the existence crack tip plasticity. Indeed, it is observed that the closer to the crack tip, the lower the τ_o values become. In this context, to be able to compare experimental results to expected values τ_o^{th} for a purely elastic behaviour, experimental values of τ_o^{exp} are taken as far as possible from the crack tip. More specifically, it was chosen to probe the second pixel from the edge of a notch, and average the value of τ_o^{exp} for the right and left cracks. The average cyclic temperature variation $\overline{\theta}$ (temperature cycle averaged over the 1000 infrared frames) measured at this peculiar pixel is plotted over two loading cycles for all 72 configurations in Fig. 14. The corresponding values of τ_o^{exp} are compared with the theoretical linear elastic effective stress ratio τ_o^{th}; results are shown in Fig. 15.

The shape of the temperature signals shown in Fig. 14 are very similar to signals observed in linear elastic simulations (Fig. 11): strong discontinuities are observed (especially for $l > 1mm$, $R_{nom} < 0$ and $f_m < 10Hz$) that resembles that of a semi-sine wave. This peculiar shape in the numerical temperature was caused by stress reversals, when the crack closes during a loading cycle. The similarity in thermal events

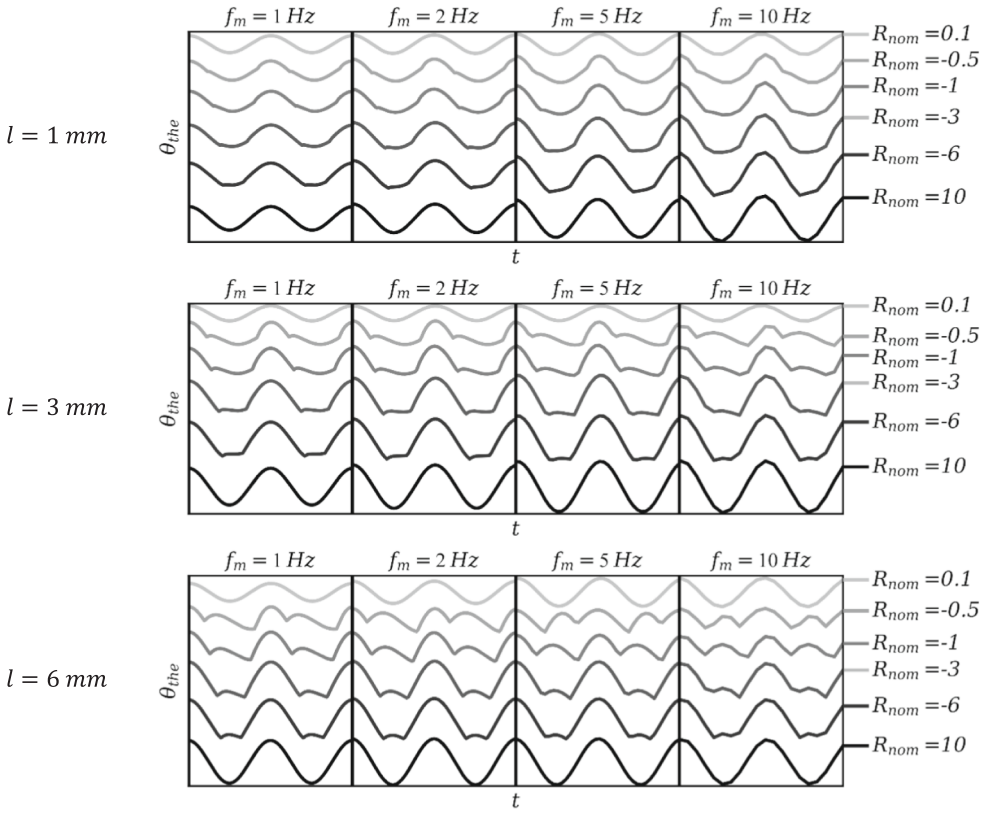

Fig. 11. Temperature linked to the thermoelastic coupling θ_{the} at the crack wake during the last two loading cycles of the numerical simulation for all 72 configurations.

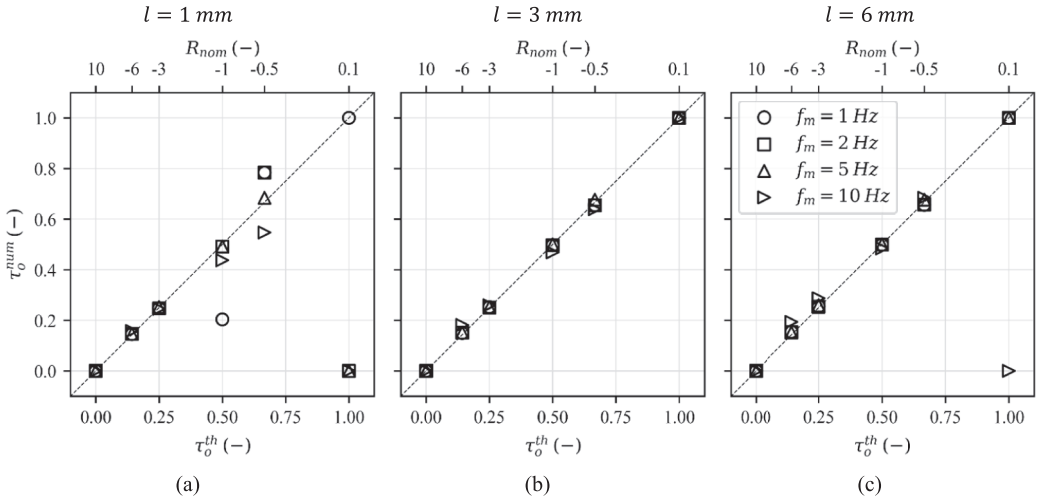

Fig. 12. Comparison of the numerical effective stress range ratio τ_o^{num} at the crack half-length to the objective theoretical value τ_o^{th} for different load ratios R_{nom} and mechanical frequencies f_m and for crack lengths $l = 1mm$ (a), $l = 3mm$ (b) and $l = 6mm$ (c).

between experiments and simulations confirms the similarity of phenomena and hence the applicability of the proposed method on experimental data.

For the short crack ($l = 1mm$, Fig. 15a), the proposed technique for effective stress range ratio measurement is put to a hard test, as shown by the scattered results. Such results could be expected since such small cracks are particularly subject to conduction effects, as discussed in §4.3.

For the medium crack ($l = 3mm$, Fig. 15b), the measured values of τ_o^{exp} seem to be in good agreement with τ_o^{th} overall.

For the long crack ($l = 6mm$, Fig. 15c), the trend of τ_o^{exp} as a function of R_{nom} is well assessed by the proposed technique. However, a consistent gap is found between the measured value τ_o^{exp} and the theoretical reference τ_o^{th}. Such a gap can be attributed to the specimen loading history (due to previous tests at different R ratios and to the crack propagation sequence) and the induced plasticity at the crack tip, hence altering the local stress state to some extent; all of these effects are not accounted for in definition of τ_o^{th}.

Overall, the estimation of a field of the effective stress range ratio τ_o^{exp} via the proposed methodology, except in the case of small cracks ($l = 1mm$) with respect to conduction effects, appears very promising.

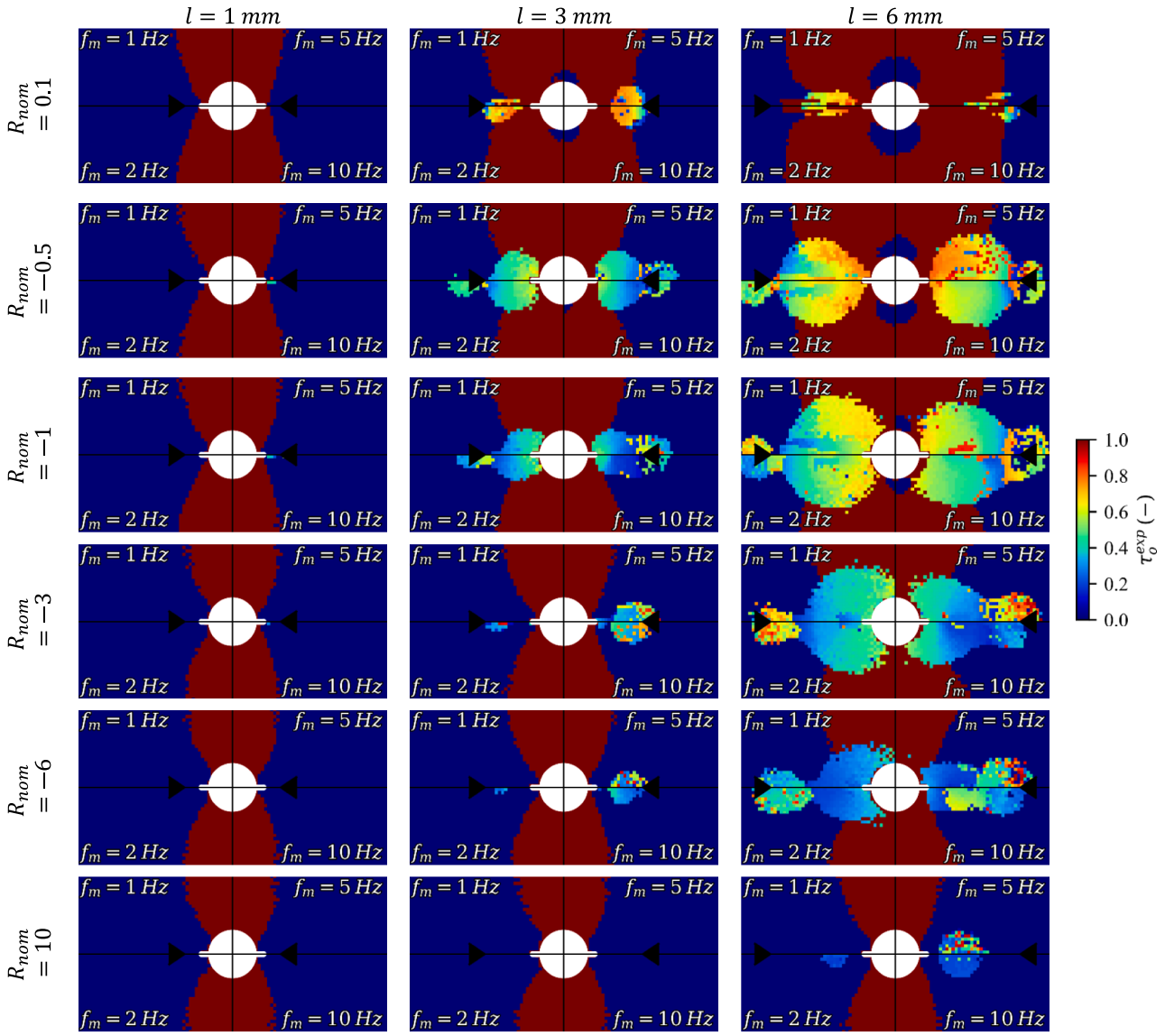

Fig. 13. Maps of the experimental effective stress range ratio τ_o^{exp} around the central notch for different load ratios R_{nom}, mechanical crack lengths l; each map is divided in four quarters to represent the τ_o field depending on the mechanical frequency f_m; the tip of the crack is indicated by a black triangle.

Indeed, for negative values of the load ratio R_{nom}, τ_o^{exp} decreases with the increase of $|R_{nom}|$, as expected. Moreover, the method allows for capturing the extent of the crack closure phenomenon along the crack wake, depending on, in particular, crack tip plasticity or process induced residual stresses.

5.2. Discussion

Experimental infrared data highlights the existence of variable closure along the crack wake. This is attributed to crack tip plasticity, altering the local stress state and hence the local stress ratio. This results in a gap between measured values τ_o^{exp} and theoretical values τ_o^{th} determined with linear elasticity assumption. Nevertheless, this does not jeopardize the applicability of the proposed method. Indeed, the temperature signal measured at the crack wake using an infrared camera is similar to that simulated in linear elasticity (Fig. 11 and Fig. 14). Singular temperature discontinuities are observed in both cases, that are caused by stress reversal during crack closure. Moreover, the analysis of spectral components of the experimental temperature at the crack tip and at the crack wake can help resolve ambiguity as to potential effect of crack tip plasticity.

The methodology proposed in this paper is based on the interpretation of higher-order harmonics in the temperature signal under cyclic loading as the indicator of crack closure. However, a significant second harmonic component in the temperature signal could also be linked to plastic behaviour of the material [35–37]. Depending on the SIF range of the studied configuration, extensive crack tip plasticity might exist and thus a sensible second-order harmonic could be measured without crack closure. To explore the influence of these phenomena in the case of the notched specimen, the average cyclic temperature $\overline{\theta}$ at the centre of the crack wake (in blue) and at the crack tip (in red) are shown in Fig. 16, as well as the corresponding magnitudes of harmonic components θ_i, with i the harmonic index, for the cases $l = 6mm$ (highest tested SIF range) and $R_{nom} < 0$. It appears that the components of order $i \geq 2$ are consistently stronger for the temperature signal at the crack wake, where there is no stress risers, than at the crack tip, where a singularity exists that could induce plastic deformation. It is especially noticeable for components of order $i \geq 3$. It tends to prove that the phenomenon observed at the crack wake is not heat dissipation linked to local plasticity nor is it caused by crack tip plasticity. This is also consistent with the work from Pitarresi and Cappello [21], where it is observed that the phase of the second harmonic component does not correspond to that expected of cyclic

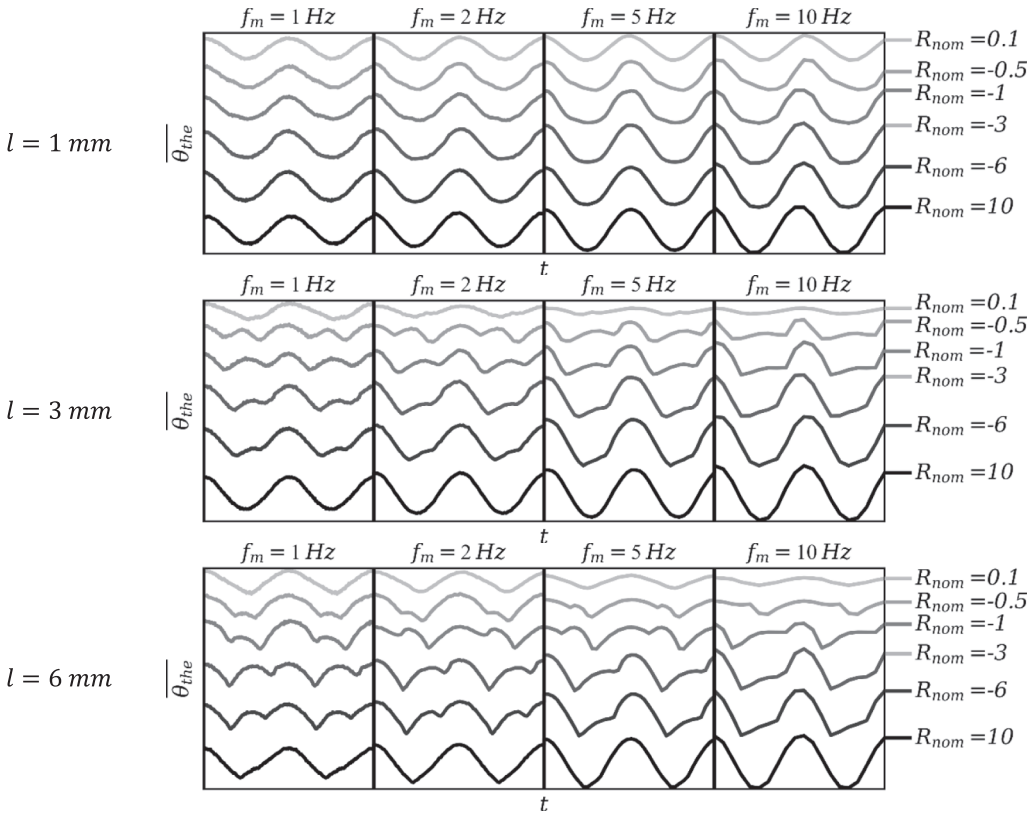

Fig. 14. Average cyclic temperature variation $\overline{\theta}$ at the crack mouth for all 72 configurations plotted over two loading cycles.

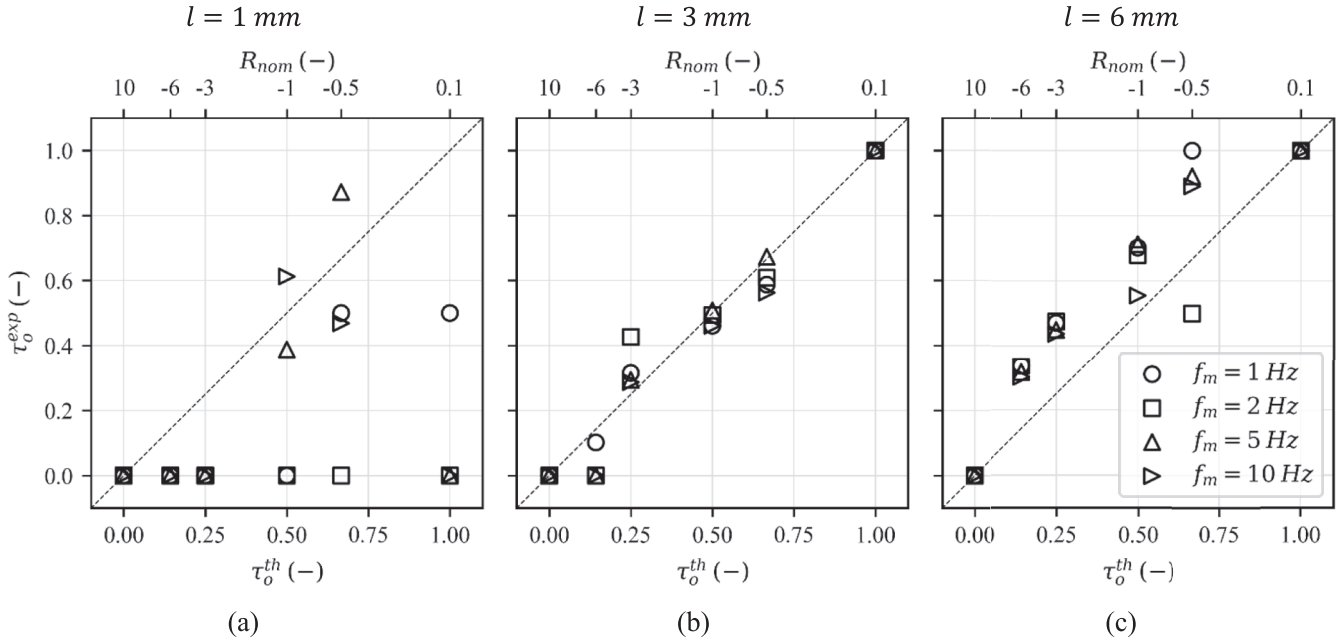

Fig. 15. Comparison of the experimental effective stress range ratio τ_o^{exp} at the crack initiation site to the theoretical value τ_o^{th} for different load ratios R_{nom} and mechanical frequencies f_m and for crack lengths $l = 1$mm (a), $l = 3$mm (b) and $l = 6mm$ (c).

plasticity. In that context, the CWT method, which detects instants when higher-order components are the most intense, solely considers the crack closure phenomenon.

5.3. Limitations to the method

The method presented in this paper relies on full-field measurement (infrared data) and requires no prior knowledge as to the position of the crack(s). In that context, it is adapted either to material samples or full-scale structures, as illustrated in [34] for a welded joint. Since the

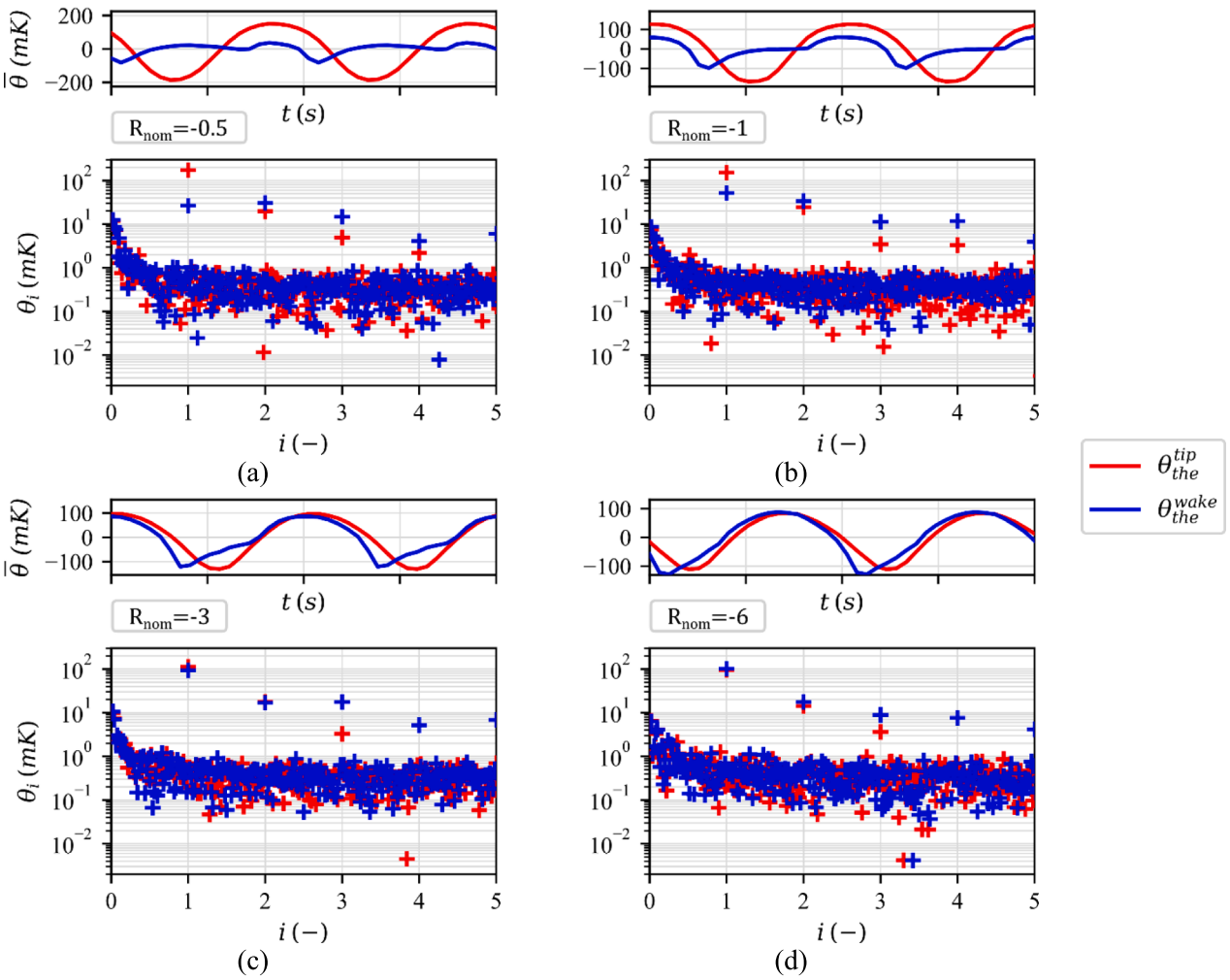

Fig. 16. Average cyclic temperature variation $\overline{\theta_{the}}$ and corresponding i^{th} harmonic magnitudes θ_i at the centre of the crack wake (θ_{the}^{wake}) and at the crack tip (θ_{the}^{tip}) for a crack length of 6 mm at $f_m = 5$Hz and at stress ratios $R_{nom} = -0.5$ (a), $R_{nom} = -1$ (b), $R_{nom} = -3$ (c) and $R_{nom} = -6$ (d).

method relies on measuring the temperature variations under cyclic loading, two limitations may exist.

The first limitation is the minimal processable stress amplitude. Indeed, for typical steel materials, a temperature variation of $1mK$ is usually obtained for a loading of $1MPa$ (see equation (4). In the present study, using the infrared camera InfraTec ImageIR 10300 with an integration time of $2200\mu s$, a noise of $25mK$ standard deviation is measured. In that context, the minimal processable stress amplitude is estimated to be $\sigma_a^{nom} \geq 15MPa$. If it is required to improve signal quality, it is possible to virtually reduce experimental noise using infrared images binning (at the expense of spatial resolution).

The second limitation is spatial resolution (*i.e.* the size of the smallest processable crack), which is dependent on conduction effects. In the present study, for the DH36 steel, it was shown that, for $f_m \leq 10Hz$, a $1mm$ long crack cannot yield satisfactory results. To mitigate conduction effects, the only available approach is to increase the mechanical frequency f_m. Although, the infrared camera sampling frequency f_c must then be chosen accordingly, to allow for the detection of stress reversals during one loading cycle. If the infrared camera's sampling frequency is too limited, the authors advise the implementation of a stroboscopic monitoring. A sufficient sampling of a loading cycle can then be obtained and allow for adequate post-processing, given that the observed crack does not propagate too much during the infrared film recording.

6. Summary and conclusions

A new methodology for automatic assessment of an effective stress range ratio related to the fatigue crack closure phenomenon was proposed in this study.

It was demonstrated that the use of conventional first harmonic TSA is not suitable for the monitoring of closing fatigue cracks. Indeed, reversals in the temperature signal due to crack closing and the existence of compressive stress can mask the presence of propagating cracks. Such temperature signal reversals correspond to the instant of closing and opening of the crack, allowing for an estimation of the effective stress range ratio τ_o.

A signal post-processing algorithm is proposed to measure the field of τ_o around the crack from temperature measurement using a limited number of user parameters. The algorithm's capability is demonstrated on the basis of perfectly elastic thermomechanical numerical simulations of a crack in a DH36 steel plate under cyclic loading in Mode I, even at low mechanical frequency and for small cracks relative to conduction effects.

The proposed algorithm is applied to experimental infrared data acquired on a notched DH36 steel plate. The measured values of τ_o^{exp} for longer cracks ($l = 3mm$ and $6mm$) are very promising: the evolution of τ_o^{exp} with respect to R_{nom} is consistent with theoretical results for a perfectly elastic case, only with a gap that is attributed to the existence of crack tip plasticity. This assumption is also supported by the obser-

vation of the variation of τ_o^{exp} along the crack wake, with smaller values towards the crack tip.

In this regard, the proposed methodology for automatic assessment of an effective stress range ratio via infrared thermography appears to be an appropriate technique for in-depth analysis of fatigue crack closure and its effect on the fatigue life of structures, as demonstrated in previous work [34]. This is an *in-situ* and quasi real time method. Consequently, this method can be adapted to study the effect of variable amplitude loading on fatigue crack growth.

CRediT authorship contribution statement

Lorenzo Bercelli: Writing – review & editing, Writing – original draft, Visualization, Validation, Supervision, Software, Resources, Methodology, Investigation, Formal analysis, Data curation, Conceptualization. **Bruno Levieil:** Writing – review & editing, Visualization, Validation, Supervision, Software, Resources, Methodology, Investigation, Formal analysis, Data curation, Conceptualization. **Cédric Doudard:** Writing – review & editing, Visualization, Validation, Supervision, Software, Resources, Methodology, Investigation, Formal analysis, Data curation, Conceptualization. **Sylvain Calloch:** Writing – review & editing, Visualization, Validation, Supervision, Software, Resources, Project administration, Methodology, Investigation, Funding acquisition, Formal analysis, Data curation, Conceptualization.

Declaration of competing interest

The authors declare that they have no known competing financial interests or personal relationships that could have appeared to influence the work reported in this paper.

Data availability

The authors are unable or have chosen not to specify which data has been used.

Acknowledgements

A part of this study belongs to the “Self-Heating” ANR-Safran-Naval Group research chair (grant no. ANR-20-CHIN-0002), involving Safran Companies, Naval Group, ENSTA Bretagne (IRDL), and Institut Pprime.

References

[1] Elber W. Fatigue crack closure under cyclic tension. Eng Fract Mech 1970;2(1):37–44. https://doi.org/10.1016/0013-7944(70)90028-7.
[2] Banerjee S. A Review of Crack Closure; 1984.
[3] Pippan R, Hohenwarter A. Fatigue crack closure: a review of the physical phenomena. Fatigue Fract Eng Mater Struct 2017;40(4):471–95. https://doi.org/10.1111/ffe.12578.
[4] Bercelli L, Levieil B, Malek B, Bridier F, Ezanno A. Use of infrared thermography to model the effective stress ratio effect on fatigue crack growth in welded T -joints. Eng Fract Mech 2023;279(September 2022):1–17. https://doi.org/10.1016/j.engfracmech.2023.109061.
[5] Barsoum Z, Barsoum I. Residual stress effects on fatigue life of welded structures using LEFM. Eng Fail Anal 2009;16(1):449–67. https://doi.org/10.1016/j.engfailanal.2008.06.017.
[6] Elber W. The Significance of Fatigue Crack Closure. In: Damage Tolerance in Aircraft Structures, ASTM International100 Barr Harbor Drive, PO Box C700, West Conshohocken, PA 19428-2959, 1971, pp. 230–242.
[7] Stoychev S, Kujawski D. Methods for crack opening load and crack tip shielding determination: a review. Fatigue Fract Eng Mater Struct 2003;26(11):1053–67. https://doi.org/10.1046/j.1460-2695.2003.00691.x.
[8] Macha DE, Corbly DM, Jones JW. On the variation of fatigue crack opening load with measurement location. Exp Mech 1979;19:207–13. https://doi.org/10.1007/BF02324983.
[9] Shin CS, Smith RA. Fatigue crack growth from sharp notches. Int J Fatigue 1985;7(2):87–93. https://doi.org/10.1016/0142-1123(85)90038-6.
[10] Chen DL, Weiss B, Stickler R. Contribution of the cyclic loading portion below the opening load to fatigue crack growth. Mater Sci Eng A 1996;208(2):181–7. https://doi.org/10.1016/0921-5093(95)10079-2.
[11] Donald JK. Introducing the compliance ratio concept for determining effective stress intensity. Int J Fatigue 1997;19(1):191–5. https://doi.org/10.1016/S0142-1123(97)00024-8.
[12] Donald K, Paris PC. An evaluation of ΔKeff estimation procedures on 6061–T6 and 2024–T3 aluminum alloys. Int J Fatigue 1999;21(1):47–57. https://doi.org/10.1016/S0142-1123(99)00055-9.
[13] Kujawski D. Fatigue Enhanced model of partial crack closure for correlation effects in aluminum alloys of R-ratio. Int J Fatigue 2001;23(2):95–102. https://doi.org/10.1016/S0142-1123(00)00085-2.
[14] Kujawski D. Correlation of long- and physically short-cracks growth in aluminum alloys. Eng Fract Mech 2001;68(12):1357–69.
[15] Kujawski D. Discussion and Comments on KOP and ΔKeff. Materials (Basel)., 2020;13(21) doi: 10.3390/ma13214959.
[16] Staal HU, Elen JD. Crack closure and influence of cycle ratio R on fatigue crack growth in type 304 stainless steel at room temperature. Eng Fract Mech 1979;11(2):275–83. https://doi.org/10.1016/0013-7944(79)90004-3.
[17] Duan QY, Li JQ, Li YY, Yin YJ, Xie HM, He W. A novel parameter to evaluate fatigue crack closure: Crack opening ratio. Int J Fatigue, 2020; 141(February), doi: 10.1016/j.ijfatigue.2020.105859.
[18] Nisitani H, Kage M. Observation of crack closure phenomena at the tip of a fatigue crack by electron microscopy. International Conference on Fracture 1977;2:1099–108. https://doi.org/10.1016/b978-0-08-022140-3.50063-x.
[19] Guvenilir A, Breunig TM, Kinney JH, Stock SR. Direct observation of crack opening as a function of applied load in the interior of a notched tensile sample of Al-Li 2090. Acta Mater 1997;45(5):1977–87. https://doi.org/10.1016/S1359-6454(96)00311-4.
[20] Wei RP, Shih TT. A study of crack closure in fatigue. Eng Fract Mech 1974;6(1):19–32.
[21] Pitarresi G, Cappello R. Evaluation of crack-closure by second harmonic thermoelastic stress analysis. Int J Fatigue 2022;vol. 164(April):107116. https://doi.org/10.1016/j.ijfatigue.2022.107116.
[22] Carteron L, Doudard C, Calloch S, Levieil B, Beaudet J, Bridier F. Naval welded joints local stress assessment and fatigue cracks monitoring with quantitative thermoelastic stress analysis. Theor Appl Fract Mech, Dec. 2020; 110(September):102792, doi: 10.1016/j.tafmec.2020.102792.
[23] Bercelli L, Doudard C, Calloch S, Le Saux V, Beaudet J. Thermometric investigations for the characterization of fatigue crack initiation and propagation in Wire and Arc Additively Manufactured parts with as-built surfaces. Fatigue Fract Eng Mater Struct, 2022; 46(1): 153:170.
[24] Ummenhofer T, Medgenberg J. On the use of infrared thermography for the analysis of fatigue damage processes in welded joints. Int J Fatigue 2009;31(1):130–7. https://doi.org/10.1016/j.ijfatigue.2008.04.005.
[25] De Finis R, Palumbo D, Di Carolo F, Ricotta M, Meneghetti G, Galietti U. Crack tip position evaluation and Paris' law assessment of a propagating crack by means of temperature-based approaches. Procedia Struct Integr 2021;39(C):528–45. https://doi.org/10.1016/j.prostr.2022.03.126.
[26] Boulanger T, Chrysochoos A, Mabru C, Galtier A. Calorimetric analysis of dissipative and thermoelastic effects associated with the fatigue behavior of steels. Int J Fatigue 2004;26(3):221–9. https://doi.org/10.1016/S0142-1123(03)00171-3.
[27] Gamot J, Lasserre T, Richard L, Neggers J, Swiergiel N, Hild F. Calibrating thermoelastic stress analysis with integrated digital image correlation: application to fatigue cracks. J Strain Anal Eng Des 2019;54(5–6):320–30. https://doi.org/10.1177/0309324719874924.
[28] Breitenstein O, Warta W, Langenkamp M. Lock-in Thermography - Basics and Use for Evaluating Electronic Devices and Materials. Berlin: Springer; 2010.
[29] Díaz FA, Yates JR, Patterson EA. Some improvements in the analysis of fatigue cracks using thermoelasticity. Int J Fatigue 2004;26(4):365–76. https://doi.org/10.1016/j.ijfatigue.2003.08.018.
[30] Díaz FA, Patterson EA, Tomlinson RA, Yates JR. Measuring stress intensity factors during fatigue crack growth using thermoelasticity. Fatigue Fract Eng Mater Struct 2004;27(7):571–83. https://doi.org/10.1111/j.1460-2695.2004.00782.x.
[31] Pitarresi G, Ricotta M, Meneghetti G. Investigation of the crack tip stress field in a stainless steel SENT specimen by means of thermoelastic stress analysis. Procedia Struct Integr 2019;18:330–46. https://doi.org/10.1016/j.prostr.2019.08.173.
[32] Camacho-reyes A, Diaz FA, Vasco-olmo JM, James MN. A higher order thermoelastic analysis of fatigue crack growth can assess crack tip shielding. no. December 2022, 2023, pp. 1–17, doi: 10.1111/ffe.13949.
[33] Du P, Kibbe WA, Lin SM. Improved peak detection in mass spectrum by incorporating continuous wavelet transform-based pattern matching. Bioinformatics 2006;22(17):2059–65. https://doi.org/10.1093/bioinformatics/btl355.
[34] Bercelli L, Guellec C, Levieil B, Doudard C, Bridier F, Calloch S. Stress ratio effect on fatigue crack growth assessment via thermoelastic stress analysis. Procedia Struct Integr 2024;57:437–44. https://doi.org/10.1016/j.prostr.2024.03.047.
[35] Krapez J-C, Pacou D, Gardette G. Lock-in thermography and fatigue limit of metals. QIRT 2000;2000:3–8. https://doi.org/10.21611/qirt.2000.051.
[36] Cappello R, Meneghetti G, Ricotta M, Pitarresi G. On the correlation of temperature harmonic content with energy dissipation in C45 steel samples under fatigue loading. Mech Mater 2022;168(January):104271. https://doi.org/10.1016/j.mechmat.2022.104271.
[37] Sakagami T, Kubo S, Tamura E, Nishimura T. Identification of plastic-zone based on double frequency lock-in thermographic temperature measurement. 11th Int. Conf. Fract. 2005, ICF11, vol. 5, 2005, pp. 3751–3756.